International Journal of Pure and Applied Mathematics

Volume 30 No. 1 2006, 71-92

IMAGE DENOISING VIA DIFFUSION MODULATION

Seongjai Kim

Department of Mathematics and Statistics
Mississippi State University
Mississippi State, MS 39762, USA
e-mail: skim@math.msstate.edu

Abstract: This article studies the method of *diffusion modulation*, a reformulation of conventional partial differential equation (PDE)-based restoration models. The reformulated models consist of three explicit components: the diffusion operator, the modulator, and the constraint term. Strategies are suggested for their appropriate choices. In particular, the *equalized net diffusion* (END) and an edge-adaptive constraint term are introduced in order to successfully restore not only fine structures but also slow transitions. The new reformulated models are highly nonlinear; a linearized numerical procedure is suggested and the resulting algorithm is analyzed for stability. The reformulation has proved to outperform conventional PDE-based models in both quality and efficiency.

AMS Subject Classification: 35K55, 65M06, 65M12
Key Words: diffusion modulation, variational approach, equalized net diffusion, edge-adaptive constraint term, PDE-based image restoration

1. Introduction

Image restoration is an important image processing (IP) step and often necessary as a pre-processing for other imaging tasks such as segmentation, registration, and compression. Thus image restoration methods, particularly for denoising, have occupied a peculiar position in IP, computer graphics, and their applications [2, 7, 17]. A considerable research has been carried out for the theoretical and computational understanding of partial differential equation (PDE)-based restoration models such as the Perona-Malik model [18], the total variation (TV) model [19], and their variants [1, 3, 4, 7, 11, 15, 16, 21].

Received: June 2, 2006

The variational approach offers a few advantages; one can usually prove convergence of the method and show a relation to a systematic probabilistic approach [7]. Diverse variants and innovative numerical schemes which prove enhanced sensitivities on important image features have been suggested to restore interesting image structures more effectively. A few examples can be found such as complex-valued diffusion processes [10], Meyer's G-norm [15] and the iterative refinement [16].

However, most of those variational models may lose fine structures and "natural look", during the restoration, due to an undesired dissipation or a tendency of converging to a piecewise constant image. In this article, we will introduce the method of *diffusion modulation* in order to overcome the drawbacks. In particular, we will study new techniques such as the *equalized net diffusion* (END) and an edge-adaptive constraint term. The objective in this article is to develop an effective (non-variational) restoration model and its numerical procedures which can restore not only fine structures but also slow transitions. Note that the set of PDEs derived from variational approaches is much smaller than the set of all available diffusion-like PDEs.

The article is organized as follows. In Section 2, we briefly review conventional PDE-based models in image denoising: variational approaches followed by their non-variational variants. Section 3 begins with analyzing sources of undesired dissipation of conventional PDE-based models and presents the END reformulation. In Section 4, numerical examples are presented to show effectiveness of the new END reformulation. Section 5 concludes our development and experiments. It has been numerically verified that the END reformulation can restore not only fine structures but also slow transitions satisfactorily, outperforming the conventional PDE-based models in both quality and efficiency. For a completeness of the article, we attach two appendices: In Appendix A, an efficient iterative procedure incorporating anisotropic diffusion difference schemes is introduced and analyzed for stability for the END model. Appendix B contains an edge-adaptive constraint term which is a function of the residual.

In this article, images are considered as discrete functions having real-values between 0 and 1 (by scaling by a factor of 1/255). After processing, they will be scaled back for the 8-bit display.

2. Preliminaries

In this section, we present a brief review of variational approaches in image denoising, followed by their non-variational variants.

2.1. Variational Approaches

Let u_0 be an observed image of the form

$$u_0 = u + g(u)v, \tag{2.1}$$

where u is the desired image and $g(u)v$ denotes the noise with v having a zero mean. For example, $g(u) = 1$ for Gaussian noise and $g(u) = \sqrt{u}$ for speckle noise in ultrasound images [13]. Then a common denoising technique is to minimize a functional of gradient:

$$u = \arg\min_u \Big\{ \int_\Omega \rho(|\nabla u|)\, d\mathbf{x} + \frac{\lambda}{2} \int_\Omega \Big(\frac{u_0 - u}{g(u)}\Big)^2 d\mathbf{x} \Big\}, \tag{2.2}$$

where Ω is the domain for the image, ρ is an increasing function (often, convex), and $\lambda \geq 0$ denotes the constraint parameter. It is often convenient to transform the minimization problem (2.2) into a differential equation, called the *Euler-Lagrange equation*, by applying the variational calculus [20]:

$$-\nabla \cdot \Big(\rho'(|\nabla u|)\frac{\nabla u}{|\nabla u|}\Big) = \lambda\, \phi(u)\, (u_0 - u), \tag{2.3}$$

where

$$\phi(u) = \frac{g(u) + (u_0 - u)g'(u)}{g(u)^3}.$$

For an edge-adaptive image denoising, it is required to hold $\rho'(x)/x \to 0$ as $x \to \infty$. For the speckle noise in ultrasound images, we have $g(u) = \sqrt{u}$ and therefore $\phi(u) = (u_0 + u)/(2u^2) \approx 1/u$; the constraint term becomes smaller at largely perturbed pixels (speckles) and as a result the resulting model can suppress speckles more effectively.

For a convenient numerical simulation of (2.3), the energy descent direction may be parameterized by an artificial time t. That is, u can be considered as an evolutionary function and the corresponding evolutionary equation can be obtained by adding $\frac{\partial u}{\partial t}$ on the left side of (2.3).

When $\rho(x) = x$ and $g(x) \equiv 1$, the model (2.3) in its evolutionary form becomes the total variation (TV) model [19]:

$$\frac{\partial u}{\partial t} - \kappa(u) = \lambda(u_0 - u), \qquad \text{(TV)} \tag{2.4}$$

where $\kappa(u)$ is the *mean curvature* defined as

$$\kappa(u) = \nabla \cdot \Big(\frac{\nabla u}{|\nabla u|}\Big).$$

It is often the case that the constraint parameter λ is set as a constant, as suggested by Rudin-Osher-Fatemi [19]. In order to find the parameter, the authors merely multiplied (2.4) by $(u_0 - u)$ and averaged the resulting equation over the whole image domain Ω. Then, for its state state,

$$\lambda = -\frac{1}{\sigma^2}\,\frac{1}{|\Omega|}\int_\Omega (u_0 - u)\,\kappa(u)\,d\mathbf{x}, \tag{2.5}$$

where σ^2 is the noise variance (in [19], λ was evaluated after applying integration by parts, which could avoid approximations of second-derivatives).

As another example of (2.3), the Perona-Malik (PM) model [18] can be obtained by setting $\rho(x) = \frac{1}{2}K^2 \ln(1 + x^2/K^2)$, for some $K > 0$, and $\lambda = 0$:

$$\frac{\partial u}{\partial t} - \nabla \cdot (c(|\nabla u|)\,\nabla u) = 0, \qquad \text{(PM)} \tag{2.6}$$

where $c(x) = \rho'(x)/x = (1 + x^2/K^2)^{-1}$. Note that for the PM model, the function ρ is strictly convex for $x < K$ and strictly concave for $x > K$ (K is a threshold). Thus the model can enhance image content of large gradient magnitudes such as edges and speckles; however, it will flatten regions of slow transitions.

Most of conventional PDE-based restoration models have shown either to converge to a piecewise constant image or to lose fine structures of the given image. Although these results are important for understanding of the current diffusion-like models, the resultant signals may not be desired in applications where the preservation of both slow transitions and fine structures is important.

2.2. Non-Variational Reformulations

The TV model tends to converge to a piecewise constant image. Such a phenomenon is called the *staircasing* effect. In order to suppress it, Marquina and Osher [14] suggested to multiply the stationary TV model by a factor of $|\nabla u|$:

$$\frac{\partial u}{\partial t} - |\nabla u|\,\kappa(u) \;=\; \lambda\,|\nabla u|\,(u_0 - u). \quad \text{(ITV)} \tag{2.7}$$

Since $|\nabla u|$ vanishes only on flat regions, its steady state is analytically the same as that of the TV model (2.4). We will call (2.7) the *improved TV* (ITV) model, as called in [17]. Such a non-variational reformulation turns out to reduce the staircasing effect successfully; however, it is yet to be improved for a better

preservation of fine structures.

To form another variant, we set $\rho(x) = x^{2-q}$, $0 \le q < 2$, in (2.3) and multiply the resulting equation by $|\nabla u|^q$, see [12]:

$$\frac{\partial u}{\partial t} - |\nabla u|^q \nabla \cdot \Big(\frac{\nabla u}{|\nabla u|^q}\Big) = \beta\,(u_0 - u), \quad \text{(CCAD)} \tag{2.8}$$

where $\beta = \lambda\,\phi(u)\,|\nabla u|^q/(2-q)$. The second-order differential operator in (2.8) turns out to be closely related to that of the PM model (2.6), in particular when $q \to 2$. Thus we will call (2.8) the *convex-concave anisotropic diffusion* (CCAD). The CCAD model can be implemented as a *stable* numerical algorithm for all $q \in [0, 2)$; see Section 5 below. It has been numerically verified that for $1 < q < 2$, the CCAD model is superior to the ITV model, a CCAD model with $q = 1$.

Now, we will consider a way of choosing a variable constraint parameter for e.g. the TV model, which has motivated the method of diffusion modulation to be presented in the next section.

As an alternative to (2.5), one can get a variable parameter $\lambda = \lambda(\mathbf{x})$ by averaging *locally*:

$$\lambda(\mathbf{x}) = -\frac{1}{\sigma_{\mathbf{x}}^2}\,\frac{1}{|\Omega_{\mathbf{x}}|}\int_{\Omega_{\mathbf{x}}} (u_0 - u)\,\kappa(u)\,d\mathbf{x},$$

where $\Omega_{\mathbf{x}}$ is a neighborhood of $\mathbf{x}$ and $\sigma_{\mathbf{x}}^2$ denotes the local noise variance measured over $\Omega_{\mathbf{x}}$. Then, the right side of the above equation can be approximated as

$$\lambda(\mathbf{x}) \approx \frac{1}{\sigma_{\mathbf{x}}^2}\,\|u_0 - u\|_{\mathbf{x}} \cdot \|\kappa(u)\|_{\mathbf{x}}, \tag{2.9}$$

where $\|\cdot\|_{\mathbf{x}}$ denotes a local average over $\Omega_{\mathbf{x}}$. Thus the TV model (2.4), when its stationary equation is scaled by $1/\|\kappa(u)\|_{\mathbf{x}}$ and regularized by a constant $\varepsilon_0 > 0$, can be rewritten as

$$\frac{\partial u}{\partial t} - \frac{1}{\|\kappa(u)\|_{\mathbf{x}} + \varepsilon_0}\,\kappa(u) = \frac{1}{\sigma_{\mathbf{x}}^2}\,\|u_0 - u\|_{\mathbf{x}}\,(u_0 - u). \tag{2.10}$$

The steady state of (2.10) must be essentially the same as that of the TV model (2.4) incorporating (2.9), when ε_0 is small. However, in practice, their numerical solutions differ a lot from each other. Note that the numerical simulation is usually terminated much earlier than reaching the steady state. The non-variational reformulation (2.10) is more *explicit and direct* than the original variational model (2.4), in the control of both diffusion and constraint.

Note that the above explicit reformulation (2.10) can be applied for various other models including the ITV model (2.7) and the CCAD model (2.8).

3. The Method of Diffusion Modulation

In this section, we will present the method of diffusion modulation, introducing an effective denoising model which consists of three components: the diffusion operator, the modulator, and the constraint term. We first analyze sources of undesired dissipation for conventional PDE-based denoising models.

3.1. Sources of Undesired Dissipation

For simplicity, we again exemplify the TV model (2.4); its corresponding noise (residual) is $v = u_0 - u$. Thus, the associated *residual equation* reads

$$\frac{\partial v}{\partial t} + \lambda\, v = -\kappa(u). \tag{3.1}$$

Although the given image u_0 is piecewise smooth and is the same as the desired image at $t = 0$, i.e., $v(t = 0) \equiv 0$, the residual at $t > 0$ becomes positive or negative at pixels where the image is concave or convex, respectively. Thus the solution of the TV model at $t > 0$, $u(t) = u_0 - v(t)$, must involve undesired dissipation wherever its curvature is nonzero; the larger the curvature is (in modulus), the more undesired dissipation occurs.

The above observation for the TV model can be applied to the general model of the form

$$\frac{\partial u}{\partial t} + Su \;=\; Q(u_0 - u), \tag{3.2}$$

where S is a diffusion operator and Q denotes a nonnegative constraint term (with appropriate choices of S and Q, the model (3.2) can express most of denoising models, including aforementioned ones). We summarize the observation as follows: *The solution of* (3.2) *must incorporate more undesired dissipation at pixels where the diffusion magnitude* $|Su|$ *is larger*. This is an unwanted property and a major source of undesired dissipation for conventional PDE-based denoising models, with which fine structures can be easily deteriorated.

3.2. The Equalized Net Diffusion (END)

In order to overcome the drawback of conventional PDE-based models, we may consider the following reformulation of (3.2), of which the diffusion operator is explicitly modulated by noise characteristics and a function of diffusion operator

itself:

$$\frac{\partial u}{\partial t} + \psi(u)\, M(Su)\, Su \;=\; R\,(u_0 - u), \tag{3.3}$$

where M is a positive function (a modulator) and R denotes an appropriate constraint term. Here $\psi(u)$ corresponds to noise characteristics, e.g., $\psi(u) = 1/\phi(u)$, where ϕ is defined as in (2.3). We will call $M(Su)\, Su$ the *net diffusion* of the model (3.3), and denote it by $N(Su)$.

The purpose of the modulator M is to suppress the undesired excessive dissipation at pixels of large diffusion magnitude $|Su|$; a strategy will be discussed below. The constraint term R can be determined to become larger at pixels where the residual reveals structural components. Such a dynamic constraint term can return important image features in the residual back to the restored image; see Section 5.

An effective modulator can be defined to impose the net diffusion *approximately equal* over a wide range of $|Su| \geq s_0 > 0$, for some s_0. However, the net diffusion function $N(s)\,(:= M(s)s)$ must be increasing and origin-symmetric. Note that the model (3.3) converges in the direction in which the net diffusion decreases (in modulus); the convergence must introduce denoising, i.e., Su becomes smaller (in modulus); which requires N to be increasing. The origin-symmetry of N implies that $N(-s) = -N(s)$, with which N becomes equally diffusive for both concavities (up and down). Such an equalized net diffusion (END) function can be defined e.g. as

$$N(s) = M(s)s = \frac{\gamma}{1 + \eta\,|s|}\, s, \tag{3.4}$$

for some positive constants η and γ. See Figure 1, where $|N(s)|$ evaluates (almost) the same values except on smooth regions (where $|s|$ is small) and therefore the function N may introduce an *equalized* net diffusion in practice. Incorporating (3.4), the model (3.3) can be rewritten as follows:

$$\frac{\partial u}{\partial t} + \psi(u)\, \frac{\gamma}{1 + \eta\,|Su|}\, Su \;=\; R\,(u_0 - u). \quad \text{(END)} \tag{3.5}$$

We will call it the *equalized net diffusion* (END) model of (3.2).

Remark. The above *method of diffusion modulation* is not completely new. The ITV model is based on such a method in which the diffusion is modulated to suppress the staircasing effect. An effective preservation of interesting image features requires more innovative ideas than the modulation involved in the ITV model. END reformulates the regularization framework in order to preserve not only fine structures but also slow transitions satisfactorily. Note that the END model is no longer conservative, i.e., there is no mathematical guarantee that

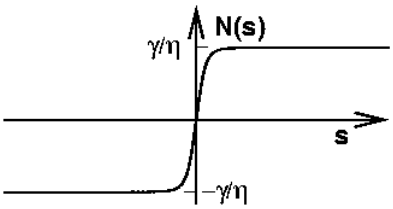

Figure 1: The net diffusion function $N(s)$ in (3.4) for some choices of η and γ

the average gray value of the input image is the same as that of the outcome. However, since the conventional PDE-based models tend to lose fine structures (Section 3.1) and easily introduce undesired dissipation, the END model turns out to produce better restored images; see numerical experiments in Section 4.

3.3. Parameters η and γ

In the remainder of the section, we will consider a strategy for the selection of appropriate η and γ. Let u^{n-1} be the solution in the last time level. Then the constants η and γ for the computation of u^n can be determined as

$$(a)\ \ N(T) = \chi \frac{\gamma}{\eta}, \quad 0 < \chi < 1\,; \qquad\qquad (b)\ \ M(T) = 1, \tag{3.6}$$

for some threshold $T > 0$. The equation (3.6.a) determines the sharpness of N near the origin; it becomes sharper, as $\chi \to 1$. On the other hand, (3.6.b) implies

$$|N(s)| < |s| \text{ for } |s| > T, \quad |N(s)| > |s| \text{ for } |s| < T. \tag{3.7}$$

Thus the net diffusion, $N(Su)$, is smaller than the original diffusion (Su) at pixels where the image content changes rapidly ($|Su| > T$), while it becomes larger in smooth regions.

The equations in (3.6) can be easily solved for η and γ, as follows:

$$\eta = \frac{\chi}{1-\chi} \cdot \frac{1}{T}, \qquad \gamma = 1 + \eta T = \frac{1}{1-\chi}. \tag{3.8}$$

Then, it follows from the above that

$$T \le |N(s)| \le \frac{\gamma}{\eta} = T \frac{1}{\chi}, \quad \text{for } |s| \ge T. \tag{3.9}$$

Thus the net diffusion on oscillatory regions ($|Su| \ge T$) can differ only by a factor of $1/\chi$. The parameter χ must be large enough to try to equalize the net diffusion on oscillatory regions; however, it should not be too large, because

otherwise the (almost flat) net diffusion will hardly be effective in denoising. We will set $\chi = 0.85 \sim 0.95$.

The threshold T must be small enough to equalize the net diffusion on every interesting oscillatory region including edges and textures. It has been numerically verified that T can be chosen to be an average of $|Su|$, S_0:

$$T = S_0 := \Big(\frac{1}{|\Omega|}\int_\Omega |Su|^2\, d\mathbf{x}\Big)^{1/2}. \tag{3.10}$$

Since the diffusion magnitude $|Su|$ evaluated from oscillatory regions is typically larger than the L^2-average S_0, the threshold T in (3.10) suffices to equalize the net diffusion for regions of fine structures. For example, for $Su = -|\nabla u|^q \nabla \cdot (\nabla u/|\nabla u|^q)$, $0 \le q < 2$, the average S_0 is often evaluated between 0.01 and 0.3 for typical natural images (the images are scaled to have values in $[0, 1]$). Let $S_0 = 0.1$ and select $\chi = 0.9$. Then it follows from (3.8), (3.9), and (3.10) that $\eta = 90$, $\gamma = 10$, and

$$0.1 \;\le\; |N(s)| \;\le\; 0.111\cdots, \quad \text{for } |s| \ge S_0 = 0.1.$$

Note that the choice of T in (3.10) keeps an average of the modulator M to be one.

The above arguments for the choice of η and γ can be summarized as follows:

1. *Select a constant* χ, $0 < \chi < 1$.
2. *Compute the* L^2*-average of* $|Su|$, S_0*:*
$$S_0 = \Big(\frac{1}{|\Omega|}\int_\Omega |Su|^2\, d\mathbf{x}\Big)^{1/2}. \tag{3.11}$$
3. *Compute the parameters* η *and* γ*:*
$$\eta = \frac{\chi}{1-\chi}\cdot\frac{1}{S_0}, \qquad \gamma = \frac{1}{1-\chi}. \tag{3.12}$$

Thus END requires the user to select only a single parameter, χ, which determines the sharpness of the net diffusion function N (one can set $\chi = 0.85 \sim 0.95$, in practice). With the resulting parameters η and γ, the average of the diffusion modulator M becomes one (independently on the selection of χ, $0 < \chi < 1$). Note that when $\chi = 0$, we have $M(s) \equiv 1$ and therefore the END model (3.5) turns out to be the conventional model (3.2).

Various numerical schemes and constraint terms can be applied for the END model (3.5). For a completeness of the article, we will present and analyze an efficient numerical procedure and an adaptive constraint term in Appendix A and Appendix B, respectively, which are somewhat straightforward variants of the author's previous results [6, 12].

(a) (b)

Figure 2: The Lenna: (a) The original image and (b) a noisy image contaminated by a Gaussian noise of PSNR=22.8 (dB)

	$q = 0.0$	$q = 0.5$	$q = 1.0$	$q = 1.4$	$q = 1.8$
CCAD[q]	27.0	27.2	27.8	28.2	28.3
END-CCAD[q]	29.8	29.8	30.1	30.2	30.3

Table 1: A PSNR analysis

4. Numerical Experiments

For numerical experiments, we select CCAD (2.8) for the basic model; in its END-incorporated model (3.5), we set $\chi = 0.9$ in (3.8). For the basic model (2.8), the parameter β is chosen from many trials to be a constant which produces the best image compared from PSNR and visual content (one may choose $\beta = \lambda|\nabla u|^q/(q-2)$, for some constant λ, as in definition; however, the result is not better than constant β for most cases). On the other hand, for the END model, we apply the adaptive constraint parameter in Section 5 with $R_0 = 0.4$ and $R_1 = 4.0$. For the numerical schemes, we choose $\theta = 1/2$ in (A.5) and $\varepsilon = 0.05$ in (A.7). The iteration is stopped along with the stopping criterion: $\|u^n - u^{n-1}\|_\infty < 0.01$. For simplicity, the noise is considered to be Gaussian: $\psi(u) \equiv 1$.

To show effectiveness of the new model and numerical schemes, we begin with the Lenna image, as depicted in Figure 2. A Gaussian noise of PSNR=22.8 (dB) is incorporated into Figure 2(b). In the following, the CCAD model with a selected q will be denoted by CCAD[q] and its corresponding END model by END-CCAD[q].

Table 1 presents PSNRs for the restored images, from Figure 2(b), by CCAD[q] and END-CCAD[q] for various q's. Note that CCAD[0] becomes the linear heat equation, while CCAD[1] is the ITV model (2.7). The CCAD model can restore a better image as q increases; it has been numerically verified that the best result can be obtained when $q = 1.5 \sim 1.9$. As one can see from the table, the END reformulation has improved the restoration quality more dramatically than different choices of basic models. Note that the PSNR of END-CCAD[0], the END-incorporated linear heat flow, is larger than those of all CCAD models not incorporating END. In practice, the END incorporation increases the computational cost by 30-50% per iteration. However, the END models have converged in 2-5 ADI iterations for all cases we have tested (including those not presented in this article); the END reformulation is often more efficient.

In Figure 3, we depict restored images and their misfits ($g-u+128$), where g denotes the original image in Figure 2(a) and u is the restored image, for three selected models considered in Table 1. As one can see from the figure, the END-CCAD[1.0] has improved the image quality a lot over CCAD[1.0]; the image quality is further improved by END-CCAD[1.8]. The END-incorporated models have restored image details very successfully. In particular, the misfit for END-CCAD[1.8] shows no significant structural components; the model has restored a desirable image satisfactorily. It should be noticed that the END reformulation improves the image quality more dramatically in visual content than in PSNR.

For the above example, better PSNRs can be obtained by selecting a relatively large β for for CCAD[q], e.g., $\beta = 1.5 \sim 2.5$; however, in the case, the algorithm may leave an observable noise in the restored image. In the above example, the constant parameter β is selected to be between 0.5 and 1. A variable constraint parameter is very important for an effective denoising.

Figure 4 contains numerical results carried out by CCAD[1.8]; in this example, we will address drawbacks of constant constraint parameters. The Zebra image is perturbed by a Gaussian noise of PSNR=18.7 (dB), as in Figure 4(b). CCAD[1.8] reaches its best PSNR (=23.1) when $\beta = 2.1$; however, the corresponding restored image still reveals an observable amount of noise as shown in Figure 4(c). When we set $\beta = 0.8$, CCAD[1.8] can obtain a reasonably well-denoised (however, looking blurrier) image having PSNR=22.3, as shown in Figure 4(d). Thus the constant constraint parameter either smears out fine structures excessively or leaves an objectionable noise into the restored image. On the other hand, when CCAD[1.8] incorporates the edge-adaptive constraint

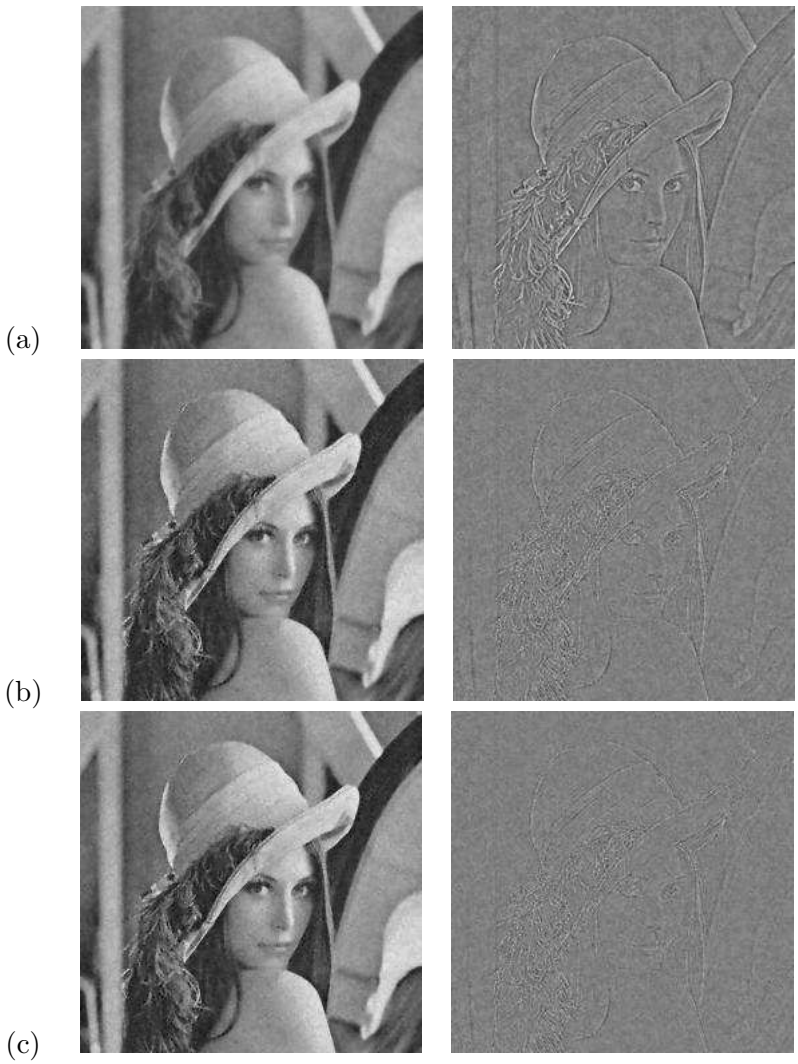

Figure 3: The restored images (left) and their corresponding misfits (right), by: (a) CCAD[1.0], (b) END-CCAD[1.0], and END-CCAD[1.8]

term in Section 5, the model results in a restored image of PSNR=23.3 as depicted in Figure 4(e). As one can find from the corresponding misfit, Figure 4(f), CCAD[1.8] has restored an acceptable image successfully when an adaptive constraint parameter is incorporated. Here the point is that the edge-adaptive constraint term (although roughly set) is at least better than the best constant parameter.

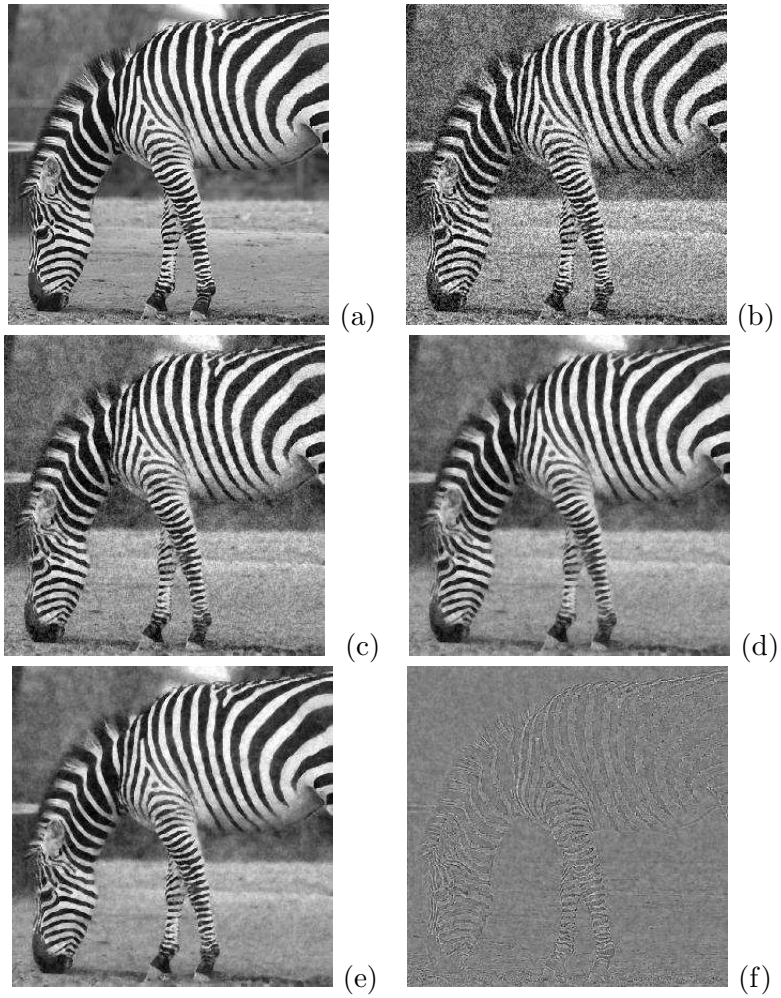

Figure 4: Zebra: (a) The original image, (b) a noisy image perturbed by a Gaussian noise of PSNR=18.7 (dB); restored images by CCAD[1.8] with (c) $\beta = 2.1$ and (d) $\beta = 0.8$; and (e) the restored image by CCAD[1.8] with the adaptive constraint term in Section 5 and (f) its corresponding misfit

The above example shows the importance of a variable constraint parameter, for an effective denoising. The END-CCAD[1.8] model results in a restored image of PSNR=24.5.

In Figure 5, we present the performance of END-CCAD[1.8] applied to the

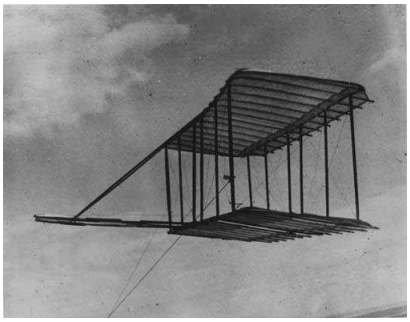
(a)
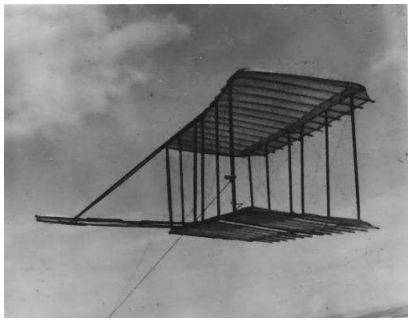
(b)

Figure 5: The Kite by Wright brothers (1900): (a) The original image and (b) a restored image by END-CCAD[1.8]

Kite that Wright brothers constructed to investigate flight principles in 1900. The original image contains a certain natural noise; it is quite challenging to reduce the noise without destroying details of the Kite, in particular thin line segments. We applied END-CCAD[1.8] for the denoising. The computation converges in two ADI iterations, producing an image as shown in Figure 5(b). As one can from the figure, the noise is well suppressed except for relatively large spots, while image details are satisfactorily preserved. Note that the adaptive constraint term is effective from the second iteration and therefore it must have helped the result slightly. Thus the superior preservation is mostly due to the END (as it can be easily verified). Another interesting feature of the END is a fast denoising in smooth regions, which in turn invokes a fast convergence overall. As shown in the second inequality in (3.7), the net diffusion of the END model in smooth regions can be much larger than that of the basic model. Indeed, since we set $\chi = 0.9$, the parameter $\gamma = 10$ and therefore $|s| < |N(s)| = \gamma|s|/(1 + \eta|s|) \leq 10|s|$, in smooth regions.

5. Conclusions

We have studied the *method of diffusion modulation* in order to overcome drawbacks of conventional PDE-based restoration models, introducing the equalized net diffusion (END). The END-incorporated model is highly nonlinear; however, it can be implemented as a stable and efficient computational algorithm by applying linearization and the ADI method. It is also *explicit* in the control of diffusion and constraint. It has been numerically verified that the newly reformulated models can restore not only fine structures but also slow transi-

tions satisfactorily, just in 2-5 ADI iterations, outperforming the conventional PDE-based restoration models in both quality and efficiency.

Acknowledgments

The work of the author is supported in part by NSF grants DMS-0312223 and DMS-0609815.

References

[1] L. Alvarez, P. Lions, M. Morel, Image selective smoothing and edge detection by nonlinear diffusion, II, *SIAM J. Numer. Anal.*, **29** (1992), 845-866.

[2] G. Aubert, P. Kornprobst, *Mathematical Problems in Image Processing*, No. 147 in Applied Mathematics Sciences, Springer-Verlag, New York (2002).

[3] M.J. Black, G. Sapiro, D.H. Marimont, D. Heeger, Robust anisotropic diffusion, *IEEE Trans. Image Processing*, **7** (1998), 421432.

[4] F. Catte, P. Lions, M. Morel, T. Coll, Image selective smoothing and edge detection by nonlinear diffusion, *SIAM J. Numer. Anal.*, **29** (1992), 182-193.

[5] Y. Cha, S. Kim, Edge-forming methods for color image zooming, *IEEE Trans. Image Process.* (2006), To Appear.

[6] Y. Cha, S. Kim, Edge-forming methods for image zooming, *J. Mathematical Imaging and Vision* (2006), To Appear.

[7] T. Chan, J. Shen, *Image Processing and Analysis*, SIAM, Philadelphia (2005).

[8] J. Douglas, Jr., J. Gunn, A general formulation of alternating direction methods, Part I: Parabolic and hyperbolic problems, *Numer. Math.*, **6** (1964), 428-453.

[9] J. Douglas, Jr., S. Kim, Improved accuracy for locally one-dimensional methods for parabolic equations, *Mathematical Models and Methods in Applied Sciences*, **11** (2001), 1563-1579.

[10] G. Gilboa, N. Sochen, Y. Zeevi, Image enhancement and denoising by complex diffusion processes, *IEEE Trans. Pattern Analysis and Machine Intelligence*, **26** (2004), 1020-1036.

[11] S. Kim, PDE-based image restoration: A hybrid model and color image denoising, *IEEE Trans. Image Processing*, **15** (2006), 1163-1170.

[12] S. Kim, H. Lim, A non-convex diffusion model for simultaneous image denoising and edge enhancement, *Electronic Journal of Differential Equations* (2006), To Appear.

[13] K. Krissian, R. Kikinis, C. F. Westin, K. Vosburgh, Speckle-constrained filtering of ultrasound images, In: *IEEE Computer Vision and Pattern Recognition or CVPR* (2005), 547-552.

[14] A. Marquina, S. Osher, Explicit algorithms for a new time dependent model based on level set motion for nonlinear deblurring and noise removal, *SIAM J. Sci. Comput.*, **22** (2000), 387-405.

[15] Y. Meyer, *Oscillating Patterns in Image Processing and Nonlinear Evolution Equations*, Volume **22** of University Lecture Series, American Mathematical Society, Providence, Rhode Island (2001).

[16] S. Osher, M. Burger, D. Goldfarb, J. Xu, W. Yin, Using geometry and iterated refinement for inverse problems (1): Total variation based image restoration, *CAM Report* #04-13, Department of Mathematics, UCLA, LA, CA 90095, 2004.

[17] S. Osher, R. Fedkiw, *Level Set Methods and Dynamic Implicit Surfaces*, Springer-Verlag, New York (2003).

[18] P. Perona, J. Malik, Scale-space and edge detection using anisotropic diffusion, *IEEE Trans. on Pattern Anal. Mach. Intell.*, **12** (1990), 629-639.

[19] L. Rudin, S. Osher, E. Fatemi, Nonlinear total variation based noise removal algorithms, *Physica D*, **60** (1992), 259-268.

[20] R. Weinstock, *Calculus of Variations*, Dover Pubilcations, Inc., New York (1974).

[21] Y.-L. You, W. Xu, A. Tannenbaum, M. Kaveh, Behavioral analysis of anisotropic diffusion in image processing, *IEEE Trans. Image Process.*, **5** (1996), 1539-1553.

Appendix A: Numerical Schemes

This appendix presents an efficient numerical procedure which incorporates anisotropic diffusion finite difference (FD) schemes for the END model (3.5) and its stability analysis.

A1: A Linearized Time-Stepping Procedure

Let Δt be the timestep size and $t^n = n\Delta t$, $n \geq 0$. Define $u^n = u(\cdot, t^n)$. For the diffusion operator, we will exemplify the CCAD model, i.e.,

$$Su = -|\nabla u|^q \nabla\cdot\Big(\frac{\nabla u}{|\nabla u|^q}\Big), \quad 0 \leq q < 2. \tag{A.1}$$

For $\ell = 1$, 2 and $m = n$, $n-1$, let $\mathcal{S}_\ell^{n-1}$ be a diffusion matrix approximating the directional diffusion operator:

$$\mathcal{S}_\ell^{n-1}\, u^m \;\approx\; -|\nabla u^{n-1}|\, \partial_{x_\ell}\Big(\frac{\partial_{x_\ell} u^m}{|\nabla u^{n-1}|}\Big) \tag{A.2}$$

(see Section 5 for the spatial numerical scheme). Let $\mathcal{S}^{n-1} = \mathcal{S}_1^{n-1} + \mathcal{S}_2^{n-1}$ and

$$F^{n-1} = \psi(u^{n-1})\, \frac{\gamma}{1 + \eta\, |\mathcal{S}^{n-1} u^{n-1}|}.$$

Define $\mathcal{A}^{n-1} = \mathcal{A}_1^{n-1} + \mathcal{A}_2^{n-1}$, where

$$\mathcal{A}_\ell^{n-1} \;:=\; F^{n-1}\, \mathcal{S}_\ell^{n-1} + \frac{1}{2}\, R^n. \tag{A.3}$$

Here R^n is the constraint term, of which an effective strategy will be considered in Section B. Then, a linearized θ-method for (3.5) can be formulated as

$$\frac{u^n - u^{n-1}}{\Delta t} \;+\; \mathcal{A}^{n-1}\, [\theta u^n + (1-\theta) u^{n-1})] \;=\; R^n\, u_0. \tag{A.4}$$

One can solve the linear system (A.4) by applying an iterative algebraic solver. However, for an efficiency reason, we employ the *alternating direction implicit* (ADI) time-stepping procedure [8, 9] for (A.4):

$$\begin{aligned} \big[1 + \theta\, \Delta t\, \mathcal{A}_1^{n-1}\big]\, u^* =& \big[1 - (1-\theta)\, \Delta t\, \mathcal{A}_1^{n-1} - \Delta t\, \mathcal{A}_2^{n-1}\big]\, u^{n-1} \\ &+ \Delta t\, R^n\, u_0, \\ \big[1 + \theta\, \Delta t\, \mathcal{A}_2^{n-1}\big]\, u^n =& u^* + \theta\, \Delta t\, \mathcal{A}_2^{n-1} u^{n-1}, \end{aligned} \tag{A.5}$$

where u^* is an intermediate solution. The spatial scheme to be presented below will result in tri-diagonal matrices $\mathcal{A}_1^{n-1}$ and $\mathcal{A}_2^{n-1}$. Thus each step of the θ-ADI procedure (A.5) can be carried out by inverting a series of tri-diagonal matrices.

A2. The Anisotropic Spatial Scheme

This subsection considers a numerical scheme for $\mathcal{S}_\ell^{n-1}$ utilized in (A.2). We will focus on the construction of $\mathcal{S}_1^{n-1}$; the same scheme can be applied to obtain $\mathcal{S}_2^{n-1}$. Let $\mathcal{D}\, u_{i-1/2,j}^{n-1}$ be a finite difference approximation of $|\nabla u^{n-1}|$ evaluated at $\mathbf{x}_{i-1/2,j}$, the mid point of $\mathbf{x}_{i-1,j}$ and $\mathbf{x}_{i,j}$. For example, a second-order scheme reads

$$\mathcal{D}\, u_{i-1/2,j}^{n-1} = \Big((u_{i,j}^{n-1} - u_{i-1,j}^{n-1})^2 + \Big[\frac{1}{2} \Big(\frac{u_{i-1,j+1}^{n-1} + u_{i,j+1}^{n-1}}{2} - \frac{u_{i-1,j-1}^{n-1} + u_{i,j-1}^{n-1}}{2} \Big) \Big]^2 \Big)^{1/2}. \quad \text{(A.6)}$$

Define

$$d_{ij,W}^{n-1} = [(\mathcal{D}\, u_{i-1/2,j}^{n-1})^2 + \varepsilon^2]^{q/2}, \quad d_{ij,E}^{n-1} = d_{i+1,j,W}^{n-1}, \quad \text{(A.7)}$$

where ε is a positive constant (small) introduced to prevent $d_{ij,W}^{n-1}$ from approaching zero. Then the differential operators in (A.2), $\ell = 1$, can be approximated as

$$-\partial_{x_1} \Big(\frac{\partial_{x_1} u^m}{|\nabla u^{n-1}|^q} \Big) \approx -\frac{1}{d_{ij,W}^{n-1}} u_{i-1,j}^m + \Big(\frac{1}{d_{ij,W}^{n-1}} + \frac{1}{d_{ij,E}^{n-1}} \Big) u_{i,j}^m - \frac{1}{d_{ij,E}^{n-1}} u_{i+1,j}^m,$$

$$|\nabla u^{n-1}|^q \approx 2 \frac{d_{ij,W}^{n-1} \cdot d_{ij,E}^{n-1}}{d_{ij,W}^{n-1} + d_{ij,E}^{n-1}}. \quad \text{(A.8)}$$

Note that the last approximation is first-order accurate. It follows from (A.2) and (A.8) that the three consecutive non-zero elements of the matrix $\mathcal{S}_1^{n-1}$ corresponding to the pixel $\mathbf{x}_{ij}$ become

$$[\mathcal{S}_1^{n-1}]_{ij} = (-s_{ij,W}^{n-1},\, 2,\, -s_{ij,E}^{n-1}), \quad \text{(A.9)}$$

where

$$s_{ij,W}^{n-1} = \frac{2\, d_{ij,E}^{n-1}}{d_{ij,W}^{n-1} + d_{ij,E}^{n-1}}, \quad s_{ij,E}^{n-1} = \frac{2\, d_{ij,W}^{n-1}}{d_{ij,W}^{n-1} + d_{ij,E}^{n-1}}. \quad \text{(A.10)}$$

It should be noticed that $s_{ij,W}^{n-1} + s_{ij,E}^{n-1} = 2$. The above non-standard numerical scheme has been successfully applied as an edge-forming formula for image zooming of arbitrary magnification factors [5, 6].

A3. Stability Analysis

Let F^{n-1} and R^n have their lower and upper bounds as

$$F_0 = \min_{i,j,n} F_{ij}^{n-1}, \quad F_1 = \max_{i,j,n} F_{ij}^{n-1}; \qquad R_0 = \min_{i,j,n} R_{ij}^n, \quad R_1 = \max_{i,j,n} R_{ij}^n.$$

The following theorem analyzes stability for the θ-method (A.4).

Theorem A.1. *Suppose that the θ-method (A.4) incorporate the numerical scheme in (A.6)-(A.10) and let*

$$(4F_1 + R_1)\,(1-\theta)\Delta t \le 1. \tag{A.11}$$

Then (A.4) holds the maximum principle and its solution satisfies

$$\|u^n - u_0\|_\infty \le \frac{4F_1}{4F_0 + R_0}\,\|u_0\|_\infty, \quad n \ge 0. \tag{A.12}$$

Proof. We will first prove the following inequality:

$$\min_{i,j} u_{0,ij} \;\le\; u_{ij}^n \;\le\; \|u_0\|_\infty, \quad n \ge 0, \tag{A.13}$$

which implies the maximum principle. The equation (A.4) at a point $\mathbf{x}_{ij}$ can be written as

$$\begin{aligned}
&[1 + (4F_{ij}^{n-1} + R_{ij}^n)\theta\Delta t]\, u_{ij}^n \\
&\quad = \theta\Delta t\, F_{ij}^{n-1}\,[s_{ij,W}^{n-1}\, u_{i-1,j}^n + s_{ij,E}^{n-1}\, u_{i+1,j}^n + s_{ij,S}^{n-1}\, u_{i,j-1}^n + s_{ij,N}^{n-1}\, u_{i,j+1}^n] \\
&\quad + (1-\theta)\Delta t\, F_{ij}^{n-1}\,[s_{ij,W}^{n-1}\, u_{i-1,j}^{n-1} + s_{ij,E}^{n-1}\, u_{i+1,j}^{n-1} + s_{ij,S}^{n-1}\, u_{i,j-1}^{n-1} + s_{ij,N}^{n-1}\, u_{i,j+1}^{n-1}] \\
&\quad + [1 - (4F_{ij}^{n-1} + R_{ij}^n)(1-\theta)\Delta t]\, u_{ij}^{n-1} + \Delta t R_{ij}^n\, u_{0,ij}.
\end{aligned} \tag{A.14}$$

Let u_{ij}^n be a local minimum. Then, it follows from (A.11) and the identity

$$s_{ij,W}^{n-1} + s_{ij,E}^{n-1} + s_{ij,S}^{n-1} + s_{ij,N}^{n-1} = 4 \tag{A.15}$$

that each of coefficients in the right side of (A.14), including the term of $u_{0,ij}$, is nonnegative and their sum becomes $1 + (4F_{ij}^{n-1} + R_{ij}^n)\theta\Delta t$. Thus, since u_{ij}^n is smaller than or equal to the neighboring values, we must have

$$u_{0,ij} \le u_{ij}^n.$$

The inequality holds for all local minima, which proves the first inequality in (A.13). The same argument can be applied for local maxima to verify the other inequality.

Now, to prove (A.12), let $\delta_{ij}^n = u_{ij}^n - u_{0,ij}$, $n \ge 0$. Then it follows from (A.14) that

$$\begin{aligned}
&[1 + (4F_{ij}^{n-1} + R_{ij}^n)\,\theta\Delta t]\,\delta_{ij}^n \\
&\quad = \theta\Delta t\, F_{ij}^{n-1}\,[s_{ij,W}^{n-1}\, u_{i-1,j}^n + s_{ij,E}^{n-1}\, u_{i+1,j}^n + s_{ij,S}^{n-1}\, u_{i,j-1}^n + s_{ij,N}^{n-1}\, u_{i,j+1}^n] \\
&\quad + (1-\theta)\Delta t\, F_{ij}^{n-1}\,[s_{ij,W}^{n-1}\, u_{i-1,j}^{n-1} + s_{ij,E}^{n-1}\, u_{i+1,j}^{n-1} + s_{ij,S}^{n-1}\, u_{i,j-1}^{n-1} + s_{ij,N}^{n-1}\, u_{i,j+1}^{n-1}] \\
&\quad - 4\Delta t\, F_{ij}^{n-1}\, u_{0,ij} + [1 - (4F_{ij}^{n-1} + R_{ij}^n)(1-\theta)\Delta t]\,\delta_{ij}^{n-1}.
\end{aligned} \tag{A.16}$$

Thus, utilizing (A.13) and (A.15), we have

$$|\delta_{ij}^n| \;\le\; \frac{4\Delta t F_1}{1+(4F_0+R_0)\,\theta\Delta t}\,\|u_0\|_\infty + \gamma_0\,\|\delta^{n-1}\|_\infty, \tag{A.17}$$

where

$$\gamma_0 = \frac{1-(4F_0+R_0)(1-\theta)\Delta t}{1+(4F_0+R_0)\,\theta\Delta t} = 1 - \frac{(4F_0+R_0)\Delta t}{1+(4F_0+R_0)\,\theta\Delta t}.$$

The inequality (A.11) also holds with F_1 and R_1 replaced respectively by F_0 and R_0; the resulting inequality can be rewritten as

$$(4F_0+R_0)\Delta t \;\le\; 1+(4F_0+R_0)\,\theta\Delta t,$$

which implies $0 \le \gamma_0 < 1$. Since $\|\delta^0\|_\infty = 0$, we can have

$$\begin{aligned} |\delta_{ij}^n| &\le \frac{4\Delta t F_1}{1+(4F_0+R_0)\,\theta\Delta t}\cdot\sum_{k=0}^{n-1}\gamma_0^k\cdot\|u_0\|_\infty \\ &\le \frac{4\Delta t F_1}{1+(4F_0+R_0)\,\theta\Delta t}\cdot\frac{1}{1-\gamma_0}\cdot\|u_0\|_\infty \;=\; \frac{4F_1}{4F_0+R_0}\,\|u_0\|_\infty, \end{aligned} \tag{A.18}$$

which completes the proof. □

The above analysis deserves a few remarks.

— The θ-method (A.4) is unconditionally stable for $\theta = 1$. When $\theta = 1/2$ (Crank-Nicolson), the stability condition reads

$$\Delta t \le \frac{2}{(4F_1+R_1)}.$$

However, in practice, it is stable for reasonable choices of the timestep size, say, $\Delta t \le 2$.

— The stability condition (A.11) holds independently on $0 \le q < 2$.

— The main diagonal of the matrix $\mathcal{S}^{n-1}$ is 4 for all $n \ge 1$, independently on both q and the image. The numerical scheme in (A.6)-(A.10), producing such a diffusion matrix, plays important roles in mathematical analysis and practical computation.

Appendix B: An Adaptive Constraint Term

The determination of the constraint parameter has been an interesting problem for PDE-based models. The basic mechanism of the PDE-based denoising is diffusion. Thus the parameter R cannot be too large; it must be small enough to introduce a sufficient amount of diffusion. On the other hand, it should be

large enough to keep the details in the image. However, in the literature, the parameter has been chosen constant for most cases; the resulting models can either smear out fine structures excessively or leave an objectionable amount of noise into the restored image.

In order to overcome the difficulty, the parameter must be set variable, more precisely, *edge-adaptive*. Our strategy toward the objective is to *allow the parameter grow wherever dissipation is excessive, keeping it small else where*. In the following, we will consider an automatic and effective numerical method for the determination of the constraint function $R(\mathbf{x}, t)$:

1. Set R as a constant:

$$R^0 = R(\mathbf{x}, 0) = R_0. \tag{B.1}$$

2. Set $R^1 = R^0$ and for $n = 2, 3, \cdots$

(2a) Compute the absolute residual and G_{Res}^{n-1}:

$$E^{n-1} = |u_0 - u^{n-1}|, \quad G_{Res}^{n-1} = \max\left(0,\, S_m(E^{n-1}) - \overline{E^{n-1}}\right), \tag{B.2}$$

where S_m is a smoother and $\overline{E^{n-1}}$ denotes the L^2-average of E^{n-1}.

(2b) Update:

$$R^n \;=\; R^{n-1} \;+\; \xi^n\, G_{Res}^{n-1}, \tag{B.3}$$

where ξ^n is a scaling factor having a property that $\xi^n \to 0$ as $n \to \infty$.

The above procedure has been motivated from the following observation. The PDE-based denoising algorithms tend to have a larger numerical dissipation near fine structures such as edges and textures. The tendency in turn makes the residual have structural components on regions where dissipation is excessive. Such structural components in the residual can be viewed as an indicator for an undesired dissipation. By adding the components (after smoothing) to the constraint parameter R, we may reduce the undesired dissipation there. It should also be noticed that from a view point of (2.10), the constraint term would better be a function of the residual.

In practice, one may wish to limit the constraint term in a prescribed interval, i.e., $R(\mathbf{x}, t) \in [R_0,\, R_1]$. Then, we can determine the scaling factor ξ^n as follows:

$$\xi^n \;=\; \frac{1}{2^{n-1}} \cdot \frac{R_1 - R_0}{\|G_{res}^{n-1}\|_\infty}, \quad n = 2, 3, \cdots. \tag{B.4}$$

Remark. The recursive update in the above adaptive constraint term has excluded the case $n = 1$, because $E^0 = |u_0 - u^0| \equiv 0$ as usual. One may try to

adjust the algorithm along with

$$E^{n-1} = \begin{cases} |\mathcal{S}^0 u_0|, & \text{for } n = 1, \\ |u_0 - u^{n-1}|, & \text{for } n \geq 2. \end{cases}$$

However, the adjustment turns out to improve the result *a little*, not much.